ADVANCED FUNCTIONAL MATERIALS
www.afm-journal.de

Enhancing Optoelectronic Properties in Phthalocyanine-Based SURMOFs: Synthesis of ABAB Linkers by Avoiding Statistical Condensation with Tailored Building Blocks

Lukas S. Langer, Mareen Stahlberger, Xiaojing Liu, Yi Luo, Niklas E. Häußermann, Puja Singhvi, Yidong Liu, Olaf Fuhr, Martin Nieger, Lars Heinke, Thomas Heine, Christof Wöll, and Stefan Bräse**

Phthalocyanine (PC)-based metal–organic frameworks (MOFs) hold substantial promise for applications in energy storage, sensing, and catalysis due to their robust stability and enhanced electron transfer capabilities. However, synthesizing phthalocyanine linkers with precise geometries presents a significant challenge, which limits their prevalence in the field. Traditional methods typically employ readily synthesized tetratopic PC linkers for realizing PC-based MOFs. In response, the study presents an innovative approach using ditopic ABAB-phthalocyanine MOF linkers. The A and B building blocks in PC synthesis are deliberately designed to circumvent issues of statistical condensation. These PC linkers are then utilized in the fabrication of zinc-based surface-anchored MOF (SURMOF) thin films. The structural and electronic properties of these SURMOFs are explored through a series of detailed experimental and computational methods, including X-ray diffraction, scanning electron microscopy (SEM), and density functional theory (DFT) calculations. UV–Vis spectroscopy reveals significant improvements in electronic absorption, thereby enhancing the material's performance in light harvesting and energy conversion. Furthermore, a photodetector built with this novel linker demonstrates high efficacy in the long-wavelength region (780 nm), highlighting its potential for cutting-edge sensing technologies.

1. Introduction

Phthalocyanines (PCs), synthetic analogues of porphyrins, consist of four isoindole subunits with 18 π-electrons.[1] These compounds are exceptionally stable and the strongly delocalized π-system in PCs, along with their adaptable metal centers, enables their application in diverse fields like dyes, pigments,[1] catalysis,[1] energy storage and harvesting,[2] and medicine.[3] Their distinct electronic structure with absorbance in the red and the near-infrared (near-IR) spectral region renders them particularly promising for photovoltaic and photodetector applications.[4] Crafting effective PC-sensitizers for photovoltaics requires synthesis of properly-functionalized PCs and the subsequent integration into devices, which typically requires the fabrication of well-defined thin films.[5] Particularly for the development of PC-based sensors, employing di- or tetratopic PC linkers to assemble metal–organic frameworks (MOFs) is a prominent strategy.[6] MOFs are crystalline porous materials, formed by linking metal nodes to organic linkers. A number of methods have been developed to deposit MOF thin films on solid substrates, including layer-by-layer approaches yielding well-ordered and oriented crystalline MOF films, commonly referred to as SURMOFs (surface-anchored MOFs).[7] Depending on the topology of the used MOF, through-space interactions can be used to further tailor the electronic

L. S. Langer, M. Stahlberger, N. E. Häußermann, S. Bräse
Institute of Organic Chemistry
Karlsruhe Institute of Technology (KIT)
Kaiserstrasse 12, 76131 Karlsruhe, Germany
E-mail: braese@kit.edu

The ORCID identification number(s) for the author(s) of this article can be found under https://doi.org/10.1002/adfm.202421693

DOI: 10.1002/adfm.202421693

X. Liu, Y. Luo, Y. Liu, L. Heinke, C. Wöll
Institute of Functional Interfaces (IFG) Karlsruhe Institute of Technology (KIT)
Kaiserstrasse 12, 76131 Karlsruhe, Germany
E-mail: christof.woell@kit.edu

Y. Luo
College of Chemistry and Molecular Sciences
Wuhan University (WHU)
Wuhan 430205, China

P. Singhvi, T. Heine
Theoretische Chemie
Technische Universität Dresden
Bergstraße 66c, König-Bau, 01062 Dresden, Germany

structure of the final molecular solid. In particular, for assembling chromophores into crystalline solids, the so-called MOF approach has been successful.[8] Depending on the particular type of MOF, the PCs are arranged into arrays spreading in two dimensions, featuring significant in-plane π-delocalization and minimal out-of-plane coupling. For appropriate MOF topologies, π–π-stacking of the PC-cores can be achieved, opening up the possibility to invoke band-structure effects like indirect bandgaps to optimize performance of PC-MOF-based devices.[9] The porous structure of the MOF maximizes the exposure of active sites (e.g., the metal PC-centers) within the material. Consequently, PC-based SURMOFs offer numerous applications in domains such as batteries,[10] sensors,[6] and catalysts.[5,11] A major obstacle in the realization of PC-based MOF thin films is the very challenging synthesis of functionalized PCs. To date, there have been limited reports on the development of PC-based MOFs. Most existing studies have employed tetratopic PCs, functionalized with -NH_2 or -OH groups, to establish framework coordination connections.[10,12] However, transitioning to linear, ditopic ABAB-PCs offers advantages, as it allows for the independent tuning of the B unit to optimize optoelectronic properties, while the A unit is specifically dedicated to anchoring the PC within the framework. One design strategy for ditopic PC-based linkers is the attachment of the carboxylic acid moieties outside of the PC-plane through conjugation to A_4-PCs with central silicon atoms.[13] While this linker design has been employed for the fabrication of Zn-based SURMOFs, the geometry of the linkers in a 3D-network hinders π–π-stacking interactions, which would be desirable to achieve specific optoelectronic properties. To achieve this, low-symmetry PC-linkers with in-plane carboxylic acid connectors are required, enabling topologies similar to those in SURMOF-2. However, this goal remains unmet due to the significant synthetic challenges in producing ABAB-type PCs. Since the synthesis of the first PC in 1907,[1] the statistical cyclotetramerization of the four monomers of aromatic *o*-dicarboxylic acid derivatives has been the predominant synthesis route, which always yields tetratopic PC-linkers of high symmetry.[14] A way to obtain PCs with other functionalities and substitution patterns is the statistical condensation of different phthalonitrile precursors. If two different phthalonitriles are used, a mixture of six regioisomers is obtained. Different approaches have been developed to improve the regioselectivity of this statistical condensation, through which PC derivatives with reduced symmetry can be obtained.[15] In the case of A_3B-type PCs, regioselectivity is controlled by the monomer concentration to selectively obtain the desired product.[16] Conversely, relatively few studies have employed statistical condensation to synthesize ABAB-type PCs. In these reports,[17] careful selection of functional groups in the precursors was crucial to achieve regioselectivity and prevent self-condensation. ABAB-type PC-based MOF-linkers have not yet been reported. In this work, we extend the method by Torres et al.[17] to selectively synthesize a Zn-metalated ditopic ABAB- PC linker, with carboxylic acid as anchoring groups, which is subsequently used to construct a novel Zn-ZnPC SURMOF structure. To the best of our knowledge, these are the first ABAB-PC MOF linkers used to successfully create the inaugural PC-based SURMOF-2 structure. The atomistic and the electronic structure of the synthesized SURMOF was characterized through a combined experimental and computational approach, involving X-ray diffraction, UV–vis absorption spectroscopy and density functional theory (DFT) calculations (**Scheme 1**).

2. Synthesis of Phthalocyanines

In the Zn-templated approach published by Torres et al., the selectivity to specifically produce ABAB-PCs stems from a careful selection of the two types of phthalonitrile precursors.[17b] One phthalonitriles contains bulky, electron-withdrawing bis(trifluoromethyl)phenyl groups at the non-peripheral positions that is essential to avoid self-condensation. The other phthalonitrile precursor can be chosen freely to implement the desired residue for further functionalization. Thus, we selected the phthalonitrile precursors for our linker synthesis accordingly. The sterically demanding 3,6-bis(trifluoromethyl)phenyl phthalonitrile **1** was synthesized as described by Torres et al. (for details, see Supporting Information).[17b] For the functionalized phthalonitrile, we chose methyl 4-(5,6-dicyano-1H-benzo[*d*]imidazol-2-yl)benzoate **2** for its linear geometry and to introduce an ester moiety that can later be saponified to afford the carboxylic acid anchoring group for the SURMOF construction. The synthesis of **2** is described in the Supporting Information. Phthalonitriles **1** and **2** were dissolved with $Zn(OAc)_2$ in a mixture of DMF and *o*-dichlorobenzene under argon atmosphere (**Scheme 2**). After heating to 175 °C for three days, a color change to deep green was detected, indicating PC-formation. The crude product was carefully purified in a series of preparative TLC runs to obtain ABAB-PC **Zn-3** in 5% yield. A crystal structure could be determined, proving the ditopic geometry of the linker. After obtaining a suitable amount of **Zn-3**, the methyl ester residues were saponified using lithium hydroxide in a mixture of water, methanol and THF. The dicarboxylic acid was precipitated with HCl and centrifuged, affording the desired ABAB-PC-based linker **Zn-4** in 66% yield.

3. Synthesis and Characterization of ABAB-Phthalocyanine-Based SURMOF

Zn-4 was assembled into **Zn-ZnPC SURMOF** using a layer-by-layer (LbL) deposition process.[18] From the different LbL variants,[7,19] the spin coating technique was employed. Deposition was carried out using quartz substrates, which were activated

O. Fuhr
Institute of Nanotechnology (INT) and Karlsruhe Nano Micro Facility (KNMFi)
Karlsruhe Institute of Technology (KIT)
Kaiserstrasse 12, 76131 Karlsruhe, Germany
M. Nieger
Department of Chemistry
University of Helsinki
P.O. Box 55 (A. I. Virtasen aukio 1), Helsinki 00014, Finland
T. Heine
Helmholtz-Zentrum Dresden-Rossendorf
Permoserstraße 15, 04318 Leipzig, Germany
S. Bräse
Institute of Biological and Chemical Systems – IBCS-FMS
Karlsruhe Institute of Technology (KIT)
Kaiserstrasse 12, 76131 Karlsruhe, Germany

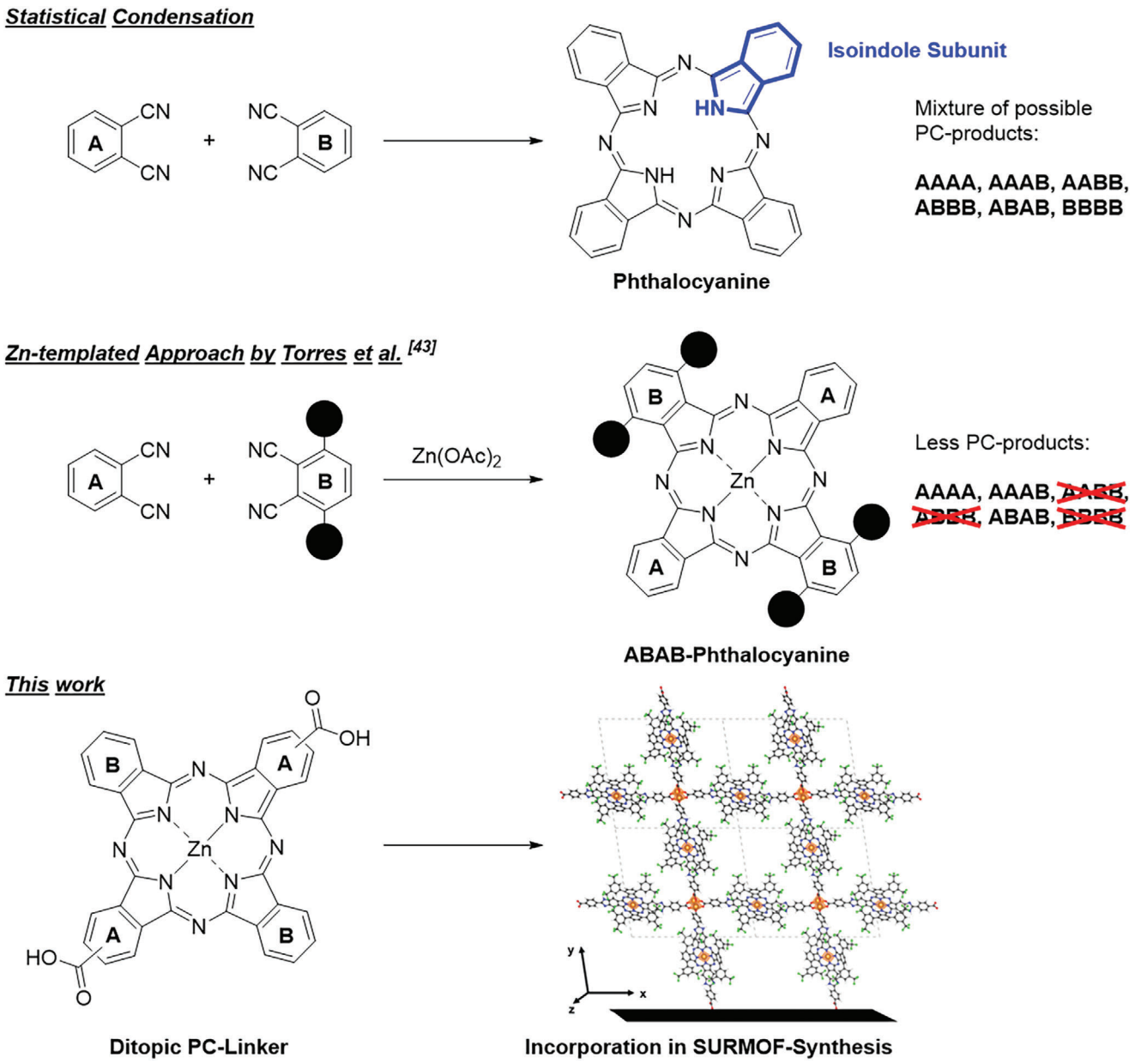

Scheme 1. Overview of statistical and selective synthesis methods for ABAB-PCs, and their application as ditopic linkers in the synthesis of PC-based SURMOFs.

by an UV-treatment prior to the deposition. Subsequently, a zinc acetate solution in ethanol and a **Zn-4** solution in DMF were used in a spin-coating apparatus at room temperature in an alternating fashion. Between each metal and linker deposition cycle, the substrates were rinsed with pure ethanol to eliminate any unbound reactants. SEM analysis revealed a flat morphology of the **Zn-ZnPC SURMOF** thin films (Figure S1, Supporting Information). The sample shows X-ray diffraction (XRD) patterns with indexes of (100), (200), and (300). The d-spacing values of the crystallographic planes were identified from the out-of-plane XRD measurements, yielding 33.05 Å. (**Figure** 1b). The simulated diffraction pattern in reciprocal space shows the possible reflection observable in out-of-plane and in-plane geometries. The 1st to 3rd order of the reflection can be observed in the out-of-plane geometry whereas only one reflection in parts of (010) can be observed in the in-plane geometry. The XRD data demonstrates consistency between the experimental and theoretical structures. For the (100) plane, the experimental 2θ value is 2.67° with a interplanar spacing of 33.05 Å, while the calculated values are 2.69° and 32.72 Å, respectively. Similarly, for the (010) plane, the experimental 2θ value is 3.09° with a d- spacing of 28.56 Å, compared to the calculated values of 3.04° and 29.03 Å. Comparable alignment is observed for the (200) and (300) peak positions.

Detailed understanding of the atomistic and the electronic structure of **Zn-ZnPC SURMOF** was obtained by performing first-principle calculations (see the Supporting Information for

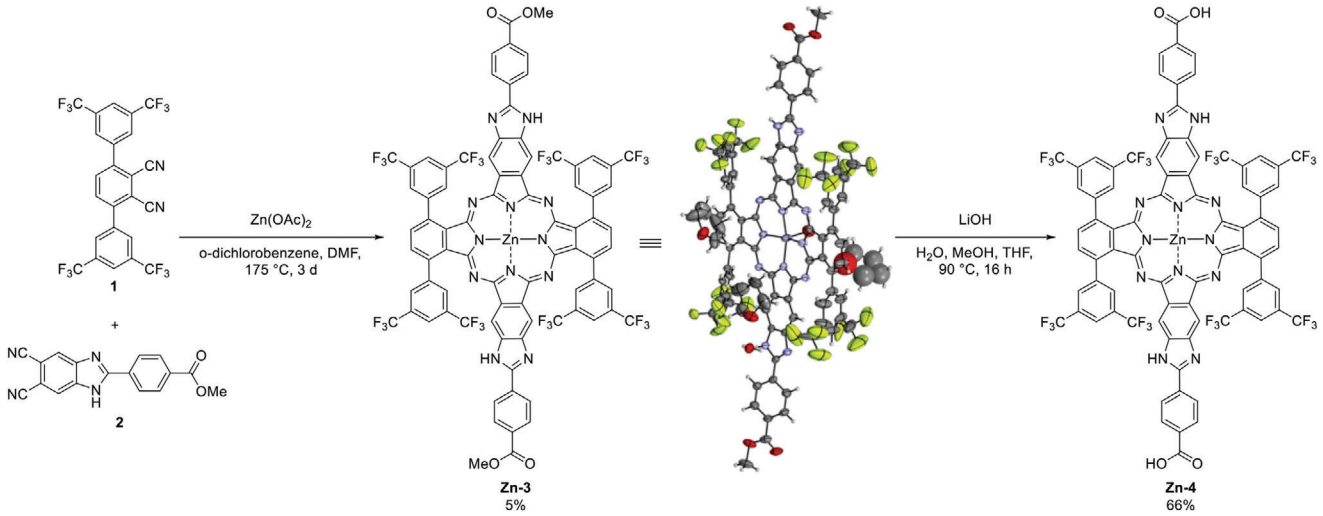

Scheme 2. Synthesis and molecular structure of ABAB-phthalocyanine **Zn-3** (displacement parameters are drawn at 50% probability level) through a Zn-templated approach and subsequent saponification to ABAB-PC-based linker **Zn-4**.

computational details). Figure 1a shows the DFT-optimized structure that consists of well-defined layers constructed from Zn^{2+} ions linked into pairs via four deprotonated **Zn-4** phthalocyanine ligands. Due to the lack of axial ligands and the closed d^{10} shell of Zn^{2+}, the $[Zn_2O_4]^{4-}$ secondary building units (SBUs) are distorted from the typical SURMOF-2 structure (with paddle-wheel conformation) toward a (quasi-)tetrahedral coordination of the Zn^{2+} ions (Figure S2, Supporting Information). Compared to the free **Zn-4** molecule, the **Zn-4** linkers in the SURMOF exhibit much more pronounced out-of-plane distortion of both the A- and the B-substituted isoindole units, and the chromophore core adopts a chair-like conformation along the sterically demanding bis(trifluoromethyl)phenyl groups (**Figure 2c**; Figure S3b,c, Supporting Information).

In contrast to the typical SURMOF-2 structure with P4 symmetry and eclipsed arrangement of the metal nodes and the linkers from adjacent layers,[20] the layers in the most stable **Zn-ZnPC SURMOF** structure are stacked in a rather inclined fashion yielding a triclinic system (Figure S3, Supporting Information). The minimum distance between the isoindole units of two adjacent **Zn-4** linkers is of the order of 7.5 Å due to the bulky bis(trifluoromethyl)phenyl substituents. Significantly shorter F•••F contacts of the order of 2.7 Å are present between the fluorine atoms in the -Ph$(CF_3)_2$ substituents from adjacent PC layers (Figure S3c, Supporting Information). The uniform tilting of the **Zn-4** linkers and the short contacts between the -Ph$(CF_3)_2$ groups give rise to the prominent (110) and (-110) diffraction peak in the simulated PXRD

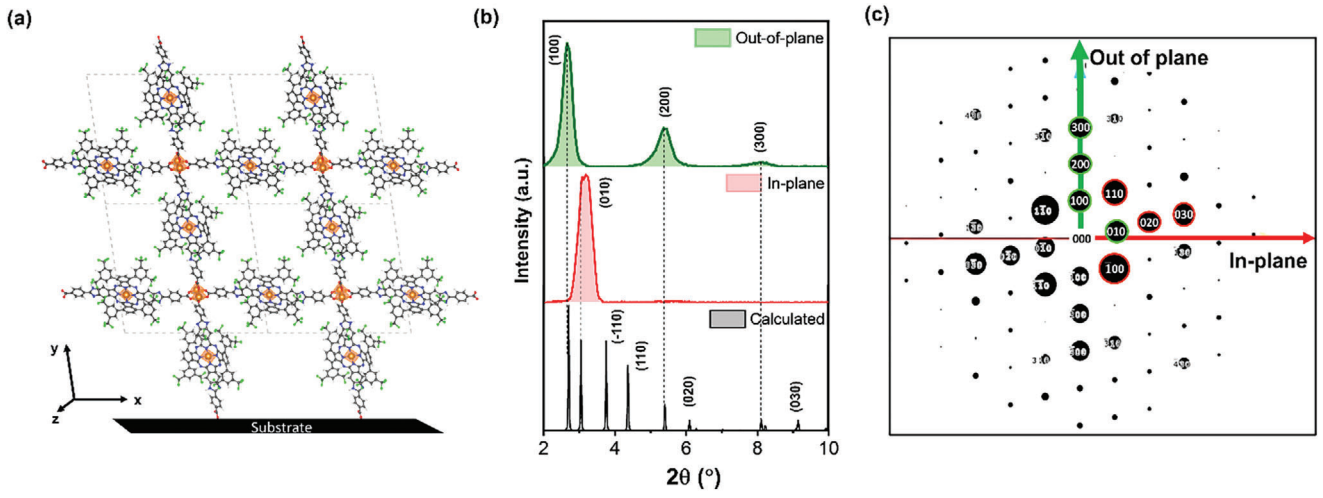

Figure 1. a) DFT-optimized **Zn-ZnPC SURMOF** structure calculated at the PBE-D3(BJ)/DZVP-MOLOPT level of theory, see Supporting Information for further computational details. Color code: H white, C grey, F green, N blue, O red, Zn orange; b) Out-of-plane, in-plane and simulated XRD patterns of **Zn-ZnPC SURMOF**; c) The simulation of a weighted reciprocal lattice based on simulated structure on quartz substrate. The out-of-plane geometry is represented by the green trace and in-plane geometry by the red trace. (Cu Kα_1 radiation used in simulation). The diffraction spots circled in green can be seen both in the experimental and simulated XRD patterns, while the red-circled diffraction spots can be seen only in the simulated XRD pattern.

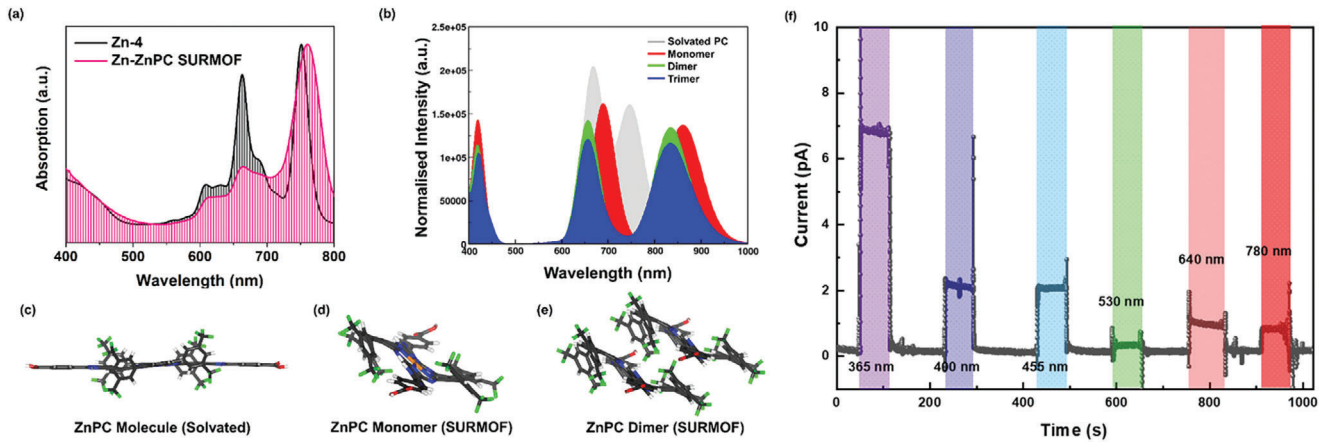

Figure 2. a) Normalized experimental UV–vis spectra of **Zn-4** (black) and **Zn-ZnPC** SURMOF (pink); b) sTDA-calculated UV–vis spectra for a ZnPC molecule (**Zn-4** in DMF solution, grey), and fragments of different size cut from the simulated **Zn-ZnPC** SURMOF structure – ZnPC monomer (red), dimer (green) and trimer (blue). sTDA-calculations at the CAM-B3LYP(D3BJ)/def2-SVP level of theory, see Supporting Information for further computational details. Broadening by Gaussian functions with FWHM = 0.15 eV is used, absorption intensities are normalized with respect to a single PC molecule; c) Stick representations of the model structures used in the calculations: **Zn-4** molecule relaxed in DFM solvent c) and monomeric d) and stacked dimeric e) **Zn-4** fragments cutout from the DFT-optimized **Zn-ZnPC SURMOF**. For details on the computational level see the SI. f) Time-dependent photocurrent response of the **Zn-ZnPC SURMOF** under chopped light irradiation of 365, 400, 455, 530, 640, and 780 nm at a bias voltage of 1 V.

for the primitive (1 × 1 × 1) cell of the **Zn-ZnPC SURMOF** (Figure 1b).

In the next step, UV–vis spectra were recorded for the **Zn-ZnPC SURMOF**. Inspection of Figure 2a reveals that the assembly of the chromophores into the crystalline lattice led to a red-shift of the prominent **Zn-4** band from 751 in solution (DMF) nm to 760 nm in SURMOF. This shift is a result of through-space interactions resulting from the shifted π–π-stacking of the PC cores. Figure 2b shows the calculated UV–vis spectra for a solvated **Zn-4** molecule (Figure 2c) and for **Zn-4** fragments of increasing size cut from the simulated solid-state structure to represent the chromophore assemblies in the **Zn-ZnPc** SURMOF (see the Supporting Information for computational details). In comparison to the experimental observations (Figure 2a), a much larger red shift of ≈110 nm is predicted for the lowest-energy band in the spectrum of the monomeric SURMOF model comprising one **Zn-4** linker with a chair-like distorted conformation (Figure 2d), with respect to that for a single molecule representing **Zn-4** in solution (Figure 2c), ≈861 nm versus 747 nm, respectively. This red shift decreases by almost 25% and is accompanied by a peak broadening if extended SURMOF models comprising two (Figure 2e) or three **Zn-4** linkers to account for interlayer interactions are used in the calculations. In the simulated spectrum of the trimer model, for instance, the first absorption peak comprises not one, but two electronic transitions with wavelengths of 843 and 820 nm (Table S3, Supporting Information). As a general conclusion, increasing the size of the finite SURMOF models yields spectra with less pronounced red-shift through-space interactions of the first absorption band and with increased intensity of this band relative to that of the second absorption band. This is in qualitative agreement with the experimental observations. A major advantage of the MOF approach is that integration of the PC chromophores into devices is straightforward. Using the LbL approach, high quality, monolithic thin films can be grown on solid substrates in a straightforward fashion. Here, we realized photodetectors with good sensitivity at wavelength of 780 nm by simply applying the LbL process to substrates with interdigitated electrodes.

For the corresponding **Zn-ZnPC** SURMOFs, the photoconductive properties were examined using two-probe direct current (DC) conduction measurements.[21] SURMOF sample was deposited on substrates with interdigitated gold electrodes, and the current was measured under photoirradiation (Figure 2f). The specific detectivity (D*) was evaluated across wavelengths of 365, 400, 455, 530, 640, and 780 nm (Table S6, Supporting Information). The results demonstrate that the highest D* is achieved at 780 nm, aligning well with the UV–vis absorption spectrum and wavelength dependence. (Figure S6, Supporting Information) Under 780 nm irradiation at an intensity of 7 mW cm^{-2}, the device exhibits a responsivity (R) of 3.45 × 10^{-13} A W^{-1} and a specific detectivity (D*) of 9.43 × 10^{5} Jones at a bias voltage of 1 V.

4. Summary and Outlook

In this study, we describe the synthesis of the first ABAB-type phthalocyanine-based MOF linker utilizing a Zn-templated condensation method. These ditopic linkers were then used to grow high-quality MOF thin films on functionized, prepatterned substrates, which demonstrated strong performance as photodetectors. The structure of the **Zn-4** MOFs was elucidated through X-ray crystallography and DFT calculations. The assembly of the **Zn-4** linkers with Zn square paddlewheel metal nodes resulted in Zn-ZnPC SURMOFs exhibiting triclinic symmetry, which contrasts with the orthorhombic structure typically observed in MOF thin films constructed from ditopic carboxylate linkers. Computational analyses revealed a deformation of the **Zn-4** linker from a flat to a chair conformation within the SURMOF matrix, supporting the bathochromic shift observed in the UV–vis absorption spectra. This congruence between computational predictions and experimental findings provides a comprehensive understanding of the structural-functional interplay within **Zn-ZnPC**

SURMOFs, establishing a foundation for designing phthalocyanine-based SURMOFs with customized properties for enhanced light harvesting and energy conversion. This work paves the way for the development of variably functionalized ABAB-type PC-MOF linkers, holding significant promise, especially in sensor technology applications.

Supporting Information

Supporting Information is available from the Wiley Online Library or from the author.

Acknowledgements

L.S.L. and M.S. contributed equally to this work. This research was funded by the Deutsche Forschungsgemeinschaft (DFG, via SPP 1928 COORNETs, via HE7036/5 and EXEC 3DMM2O–EXC-2082/1–390761711). The authors thank ZIH Dresden and Paderborn Centre for Parallel Computing (PC^2) for the use of computational resources. The authors thank Dr. Nina Vankova for fruitful discussions.

Open access funding enabled and organized by Projekt DEAL.

Conflict of Interest

The authors declare no conflict of interest.

Data Availability Statement

The data that support the findings of this study are available from the corresponding author upon reasonable request.

Keywords

light harvesting, metal–organic frameworks, photodetection, phthalocyanines, statistical condensation

Received: November 9, 2024
Revised: December 23, 2024
Published online:

[1] a) A. Braun, J. Tcherniac, *Ber. Dtsch. Chem. Ges.* **1907**, *40*, 2709; b) H. J. Wagner, R. O. Loutfy, C.-K. Hsiao, *J. Mater. Sci.* **1982**, *17*, 2781; c) R. Christie, A. Abel, *Phys. Sci. Rev.* **2021**, *6*, 671; d) S. Yang, Y. Yu, X. Gao, Z. Zhang, F. Wang, *Chem. Soc. Rev.* **2021**, *50*, 12985.

[2] a) A. Kumar, V. Kumar Vashistha, D. Kumar Das, *Coord. Chem. Rev.* **2021**, *431*, 213678; b) M. Urbani, M.-E. Ragoussi, M. K. Nazeeruddin, T. Torres, *Coord. Chem. Rev.* **2019**, *381*, 1.

[3] a) P.-C. Lo, M. S. Rodríguez-Morgade, R. K. Pandey, D. K. P. Ng, T. Torres, F. Dumoulin, *Chem. Soc. Rev.* **2020**, *49*, 1041; b) B.-D. Zheng, Q.-X. He, X. Li, J. Yoon, J.-D. Huang, *Coord. Chem. Rev.* **2021**, *426*, 213548.

[4] a) B. H. Lessard, *ACS Appl. Mater. Int.* **2021**, *13*, 31321; b) C. G. Claessens, U. Hahn, T. Torres, *Chem. Rec.* **2008**, *8*, 75; c) C. V. Kumar, G. Sfyri, D. Raptis, E. Stathatos, P. Lianos, *RSC Adv.* **2015**, *5*, 3786; d) P. F. Siles, T. Hahn, G. Salvan, M. Knupfer, F. Zhu, D. R. T. Zahn, O. G. Schmidt, *Nanoscale* **2016**, *8*, 8607; e) Y. Matsuo, K. Ogumi, I. Jeon, H. Wang, T. Nakagawa, *RSC Adv.* **2020**, *10*, 32678.

[5] a) W. Jiang, S. Zhang, Z. Wang, F. Liu, T. Low, *Nano Lett.* **2020**, *20*, 1959; b) J. Liu, Q. Sun, Q. Ye, J. Chen, Y. Wu, Y. Ge, L. Zhang, Z. Yang, J. Qian, *ACS Sustainable Chem. Eng.* **2024**, *12*, 4779; c) R. K. Parashar, P. Jash, M. Zharnikov, P. C. Mondal, *Angew. Chem., Int. Ed.* **2024**, *63*, 202317413; d) A. Sukhikh, D. Klyamer, D. Bonegardt, T. Basova, *Int. J. Mol. Sci.* **2023**, *24*, 2034; e) M. Wang, H. Shi, P. Zhang, Z. Liao, M. Wang, H. Zhong, F. Schwotzer, A. S. Nia, E. Zschech, S. Zhou, S. Kaskel, R. Dong, X. Feng, *Adv. Funct. Mater.* **2020**, *30*, 2002664; f) L. Wei, M. D. Hossain, G. Chen, G. A. Kamat, M. E. Kreider, J. Chen, K. Yan, Z. Bao, M. Bajdich, M. B. Stevens, T. F. Jaramillo, *J. Am. Chem. Soc.* **2024**, *146*, 13377; g) J.-D. Yi, D.-H. Si, R. Xie, Q. Yin, M.-D. Zhang, Q. Wu, G.-L. Chai, Y.-B. Huang, R. Cao, *Angew. Chem., Int. Ed.* **2021**, *60*, 17108.

[6] a) D. Klyamer, R. Shutilov, T. Basova, *Sensors* **2022**, *22*, 895; b) S. Lu, H. Jia, M. Hummel, Y. Wu, K. Wang, X. Qi, Z. Gu, *RSC Adv.* **2021**, *11*, 4472; c) J. Peng, L. Wei, Y. Liu, W. Zhuge, Q. Huang, W. Huang, G. Xiang, C. Zhang, *RSC Adv.* **2020**, *10*, 36828; d) M. Wang, Z. Zhang, H. Zhong, X. Huang, W. Li, M. Hambsch, P. Zhang, Z. Wang, P. S. Petkov, T. Heine, S. C. B. Mannsfeld, X. Feng, R. Dong, *Angew. Chem., Int. Ed.* **2021**, *60*, 18666; e) Z. Zeng, X. Fang, W. Miao, Y. Liu, T. Maiyalagan, S. Mao, *ACS Sens.* **2019**, *4*, 1934.

[7] J. Liu, C. Wöll, *Chem. Soc. Rev.* **2017**, *46*, 5730.

[8] R. Haldar, L. Heinke, C. Wöll, *Adv. Mater.* **2020**, *32*, 1905227.

[9] J. Liu, W. Zhou, J. Liu, I. Howard, G. Kilibarda, S. Schlabach, D. Coupry, M. Addicoat, S. Yoneda, Y. Tsutsui, T. Sakurai, S. Seki, Z. Wang, P. Lindemann, E. Redel, T. Heine, C. Wöll, *Angew. Chem., Int. Ed.* **2015**, *54*, 7441.

[10] a) F. Wang, Z. Liu, C. Yang, H. Zhong, G. Nam, P. Zhang, R. Dong, Y. Wu, J. Cho, J. Zhang, X. Feng, *Adv. Mater.* **2020**, *32*, 1905361; b) H. Nagatomi, N. Yanai, T. Yamada, K. Shiraishi, N. Kimizuka, *Chem. - Eur. J.* **2018**, *24*, 1806.

[11] H. Zhong, K. H. Ly, M. Wang, Y. Krupskaya, X. Han, J. Zhang, J. Zhang, V. Kataev, B. Büchner, I. M. Weidinger, S. Kaskel, P. Liu, M. Chen, R. Dong, X. Feng, *Angew. Chem., Int. Ed.* **2019**, *58*, 10677.

[12] a) H. Jia, Y. Yao, J. Zhao, Y. Gao, Z. Luo, P. Du, *J. Mater. Chem. A* **2018**, *6*, 1188; b) R. Matheu, E. Gutierrez-Puebla, M. Á. Monge, C. S. Diercks, J. Kang, M. S. Prévot, X. Pei, N. Hanikel, B. Zhang, P. Yang, O. M. Yaghi, *J. Am. Chem. Soc.* **2019**, *141*, 17081.

[13] a) H. Chen, L. Martín-Gomis, Z. Xu, J. C. Fischer, I. A. Howard, D. Herrero, V. Sobrino-Bastán, Á. Sastre-Santos, R. Haldar, C. Wöll, *Phys. Chem. Chem. Phys.* **2023**, *25*, 19626; b) R. Haldar, Z. Fu, R. Joseph, D. Herrero, L. Martín-Gomis, B. S. Richards, I. A. Howard, A. Sastre-Santos, C. Wöll, *Chem. Sci.* **2020**, *11*, 7972.

[14] N. B. McKeown, in *The Porphyrin Handbook*, (Eds.: K. M. Kadish, K. M. Smith, R. Guilard), Academic Press, Amsterdam **2003**, pp. 61–124.

[15] M. S. Rodríguez-Morgade, G. de la Torre, T. Torres, in *The Porphyrin Handbook*, (Eds.: K. M. Kadish, K. M. Smith, R. Guilard), Academic Press, Amsterdam, **2003**, pp. 125–160.

[16] a) B. Sezer, M. K. Şener, A. Koca, A. Erdoğmuş, U. Avcıata, *Synth. Met.* **2010**, *160*, 2155; b) F. Yuksel, D. Atilla, V. Ahsen, *Polyhedron* **2007**, *26*, 4551; c) W. Duan, P.-C. Lo, L. Duan, W.-P. Fong, D. K. P. Ng, *Bioorg. Med. Chem.* **2010**, *18*, 2672; d) A. Y. Tolbin, V. E. Pushkarev, E. V. Shulishov, A. V. Ivanov, L. G. Tomilova, N. S. Zefirov, *Mendeleev Commun.* **2005**, *15*, 24.

[17] a) T. P. Forsyth, D. B. G. Williams, A. G. Montalban, C. L. Stern, A. G. M. Barrett, B. M. Hoffman, *J. Org. Chem.* **1998**, *63*, 331; b) E. Fazio, J. Jaramillo-García, G. de la Torre, T. Torres, *Org. Lett.* **2014**, *16*, 4706; c) N. Kobayashi, T. Ashida, T. Osa, *Chem. Lett.* **2006**, *21*, 2031; d) N. Kobayashi, T. Ashida, T. Osa, H. Konami, *Inorg. Chem.* **1994**, *33*, 1735.

[18] X. Liu, A. Mazel, S. Marschner, Z. Fu, M. Muth, F. Kirschhöfer, G. Brenner-Weiss, S. Bräse, S. Diring, F. Odobel, R. Haldar, C. Wöll, *ACS Appl. Mater. Int.* **2021**, *13*, 57768.
[19] D.-H. Chen, H. Gliemann, C. Wöll, *Chem. Phys. Rev.* **2023**, *4*, 011305.
[20] a) R. Haldar, K. Batra, S. M. Marschner, A. B. Kuc, S. Zahn, R. A. Fischer, S. Bräse, T. Heine, C. Wöll, *Chem. - Eur. J.* **2019**, *25*, 7847; b) J. Liu, B. Lukose, O. Shekhah, H. K. Arslan, P. Weidler, H. Gliemann, S. Bräse, S. Grosjean, A. Godt, X. Feng, K. Müllen, I.-B. Magdau, T. Heine, C. Wöll, *Sci. Rep.* **2012**, *2*, 921.
[21] a) Y.-B. Tian, N. Vankova, P. Weidler, A. Kuc, T. Heine, C. Wöll, Z.-G. Gu, J. Zhang, *Adv. Sci.* **2021**, *8*, 2100548; b) X. Liu, M. Kozlowska, T. Okkali, D. Wagner, T. Higashino, G. Brenner-Weiß, S. M. Marschner, Z. Fu, Q. Zhang, H. Imahori, S. Bräse, W. Wenzel, C. Wöll, L. Heinke, *Angew. Chem., Int. Ed.* **2019**, *58*, 9590; c) C. Li, H. Schopmans, L. Langer, S. Marschner, A. Chandresh, J. Bürck, Y. Tsuchiya, A. Chihaya, W. Wenzel, S. Bräse, M. Kozlowska, L. Heinke, *Angew. Chem., Int. Ed.* **2023**, *62*, 202217377.